

Strange velocities in the equatorial ejecta of η Carinae^{*}

Torgil Zethson¹, Sveneric Johansson¹, Kris Davidson², Roberta M. Humphreys², Kazunori Ishibashi², and Dennis Ebbets³

¹ Department of Physics, Lund University P.O. Box 118, S-22100 Lund, Sweden (torgil.zethson; sveneric.johansson@fysik.lu.se)

² Astronomy Department, University of Minnesota 116 Church St. SE, Minneapolis, MN 55455, USA

(kd@ea.spa.umn.edu; roberta@isis.spa.umn.edu; bish@astro.spa.umn.edu)

³ Ball Aerospace P.O. Box 1062, Boulder, CO 80306, USA (debbets@ball.com)

Received 10 September 1998 / Accepted 22 December 1998

Abstract. We report HST/HRS observations of gas that appears to have been ejected in the equatorial zone of η Carinae. Some of the observed emission lines are produced by Fe II fluorescence processes, which, for unknown reasons, are uniquely intense near η Carinae. Surprisingly low velocities are found, most likely representing ejection events hundreds of years before the well-known Great Eruption of the 1840's. Alternative interpretations are possible with different geometrical assumptions, but they seem less straightforward and imply a different set of novel problems. The observed velocities less than 100 km s^{-1} must be hints concerning the physical nature of η Carinae; we propose one speculative scenario, combining the effects of rotation and a modified Eddington limit. The strong fluorescent emission lines occur only in the slowest gas, a result that we cannot yet explain. Altogether, these data pose a number of serious theoretical questions and clues, involving remarkably slow ejection speeds, formation of distinct dense condensations in the ejecta, and peculiarly intense radiative excitation of certain emission lines.

Key words: line: identification – stars: individual: η Carinae – stars: variables: general – ISM: jets and outflows

1. Introduction

The “Homunculus Nebula” formed by ejecta from η Carinae is one of the most remarkable of known bipolar objects, with several attributes that are not understood even in a rudimentary sense. The complex structure near the midplane is especially puzzling; it resembles a disk of equatorial ejecta, but lacks azimuthal symmetry and includes many dense, narrow radial “spokes” or “rays” or “jets” whose origins are unclear (Duschl et al. 1995; Davidson et al. 1997; Davidson and Humphreys 1997; Morse et al. 1998). Here we report HST observations that

add a new element of complexity to the situation: unexpectedly low velocities in the central midplane region may indicate the presence of slow-moving material ejected before the famous “Great Eruption” seen 150 years ago. Moreover, the peculiar fluorescent Fe II emission features, which are astonishingly bright near η Carinae (Johansson et al. 1996, 1998), seem restricted to the slowest velocity components.

The spectroscopic observations described in this paper were planned with two main goals in mind. First, we sought ultraviolet data on certain fluorescent processes that are more intense near η Carinae than in any other known object (Johansson & Hamann 1993; Johansson et al. 1996, 1998); this complex topic will be discussed in a later paper. The second and apparently simpler goal concerned the age of the equatorial ejecta. Most authors have naturally assumed that the bipolar lobes and the equatorial disk were all produced in the Great Eruption observed in the 1840's (see, e.g., Currie et al. 1996). However, various clues suggest that at least some of the equatorial debris were ejected in a different event about 50 years later (see Sect. 4.2 of Davidson & Humphreys 1997; Duschl et al. 1995; Davidson et al. 1997). We hoped that radial velocities would provide a simple test of this question. For instance, at one of our target positions, 1.3 arcsec northwest of the central star, the apparent radial velocity was expected to be close to -135 km s^{-1} if the gas was ejected in the 1840's, or almost -200 km s^{-1} if it is 50 years younger. The HST's Goddard High Resolution Spectrograph (HRS) provided adequate spatial and spectral resolution for such a test. After our observations were planned, Smith & Gehrz (1998) re-examined available positional data from the years 1915 to 1995 and concluded that the most prominent equatorial features were ejected at the later date, in the 1890's. Therefore we expected to find velocities of about -200 km s^{-1} in the HRS data at that location, and faster at other places farther from the star.

Much to our surprise, however, no velocity components near -200 km s^{-1} appear in the HRS data, and most of the observed velocities are slower than -100 km s^{-1} . In the simplest, most obvious interpretation, these are remnants of outbursts spanning an interval of several hundred years before the Great Eruption. If so, then their remarkably low speeds may be clues to the nature of the unstable star. In such a case the UV emission lines reported in this paper cannot represent the same material as the

Send offprint requests to: T. Zethson

^{*} Based on observations with the NASA/ESA Hubble Space Telescope, and supported by grant numbers GO-6041 and GO-6501 from the Space Telescope Science Institute. The STScI is operated by the Association of Universities for Research in Astronomy, Inc., under NASA contract NAS5-26555.

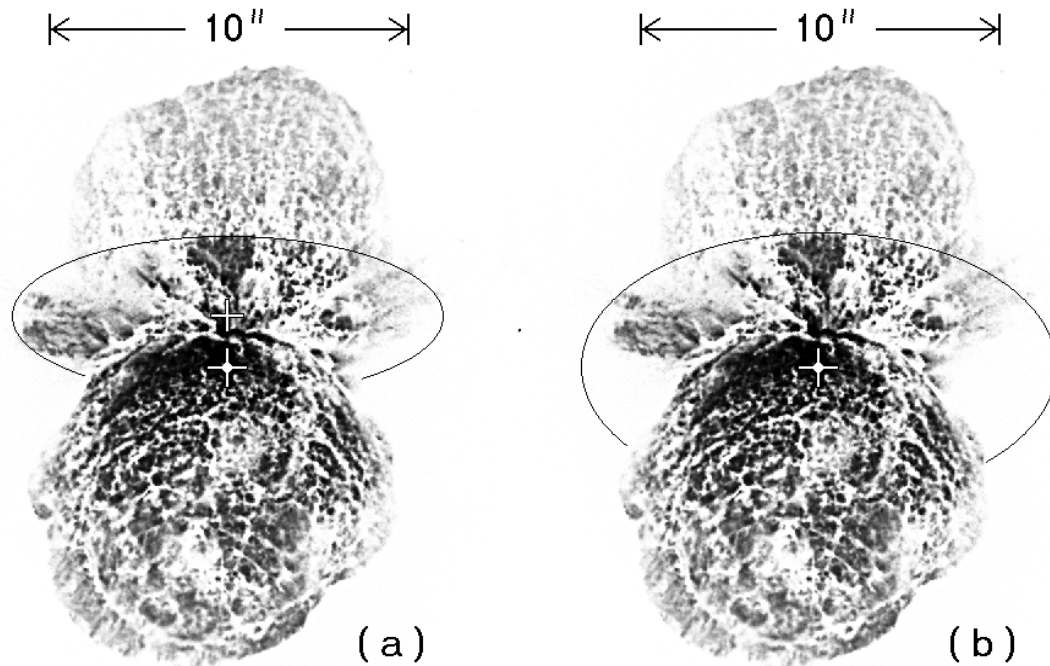


Fig. 1a and b. The “Homunculus” bipolar nebula, shown with northwest at the top and northeast at the left side. The ellipses demonstrate that the apparent outline of the equatorial ejecta is not straightforward to interpret, as discussed in the text.

condensations that Smith & Gehrz discussed. (The latter are generally farther from the central star, and are seen mainly as reflected light in visual-wavelength images.) Alternative interpretations are also interesting, as discussed in Sect. 5 below.

Sect. 2 of this paper contains remarks about the spatial orientation of the observed velocities; Sect. 3 is an account of our observations; the observed emission features and velocity components are described in Sect. 4; and possible explanations are outlined in Sect. 5.

2. Concerning the large-scale geometry of the equatorial ejecta

The direction of motion of the observed gas is critical for the goals of this paper. However, available images present a little-noted ambiguity regarding the orientation of the midplane ejecta of η Carinae.

Denote by ψ the angle between our line of sight and the velocity of an observed gaseous condensation (measured relative to the central star), so that $\psi = 0$ for motion directly toward us. Let t be the time elapsed since the gas was ejected from the central star; assume that the gas is not significantly decelerated; let b represent the apparent *projected* linear distance of the gas from the star; and denote the star’s apparent radial velocity by V_{system} . (Probably $V_{system} \sim -7 \text{ km s}^{-1}$ heliocentric, see Davidson et al. 1997.) Then the apparent radial velocity of the gas is

$$V_{obs} = V_{system} - \frac{b}{t \tan \psi}.$$

As an approximation, suppose that the bipolar Homunculus is axially symmetric with inclination i defined like the axis of a

binary star orbit, i.e., $i = 90^\circ$ would correspond to an “edge-on” view of the equatorial midplane. The value of i appears to be roughly 55° , based on observed radial velocities in the bipolar lobes and on the projected location of the central star relative to the apparent lobe edges (see refs. cited in Sect. 4 of Davidson & Humphreys 1997, and in Davidson et al. 1997). Our main HRS target positions are close to the projection of the bipolar axis on the plane of the sky (see Fig. 2). Therefore, if the observed gas is moving in the equatorial midplane of the Homunculus, then its direction of motion away from the star should satisfy $\psi \approx 90^\circ - i \approx 35^\circ$.

However, Fig. 1 shows that *the appearance of the equatorial ejecta does not match a simple model with $i \approx 55^\circ$* . The outline sketched in Fig. 1a has two surprising characteristics: its center definitely does not coincide with the star, and the ellipse is too flattened for $i \approx 55^\circ$. The former discrepancy, at least, has seldom been noticed, probably because the star’s location is not obvious in most printed images. We can suggest three alternative explanations. (1) Conceivably the outline in Fig. 1a is correct and the “equatorial skirt” is really a flat cone, somewhat tilted relative to the bipolar axis. Then one finds the direction of motion on the nearest side to be $\psi \approx 38^\circ$, not much different from the 35° expected in a planar model with $i \approx 55^\circ$. (2) Perhaps the true outline is a circle with $i \approx 55^\circ$ as shown in Fig. 1b, but the far side is hidden by dust. However, this idea does not explain why two large areas on each side of the “waist” of the Homunculus appear as empty in infrared images as they do at visual wavelengths (cf. Smith et al. 1998; Morse et al. 1998; Duschl et al. 1995). These areas are within the elliptical outline marked in Fig. 1b, and represent large fractions of the hypothetical disk region; yet there is no sign of material there.

Table 1. Locations observed. Each position is the center of the spectrograph aperture, relative to the central star at the time of observation.

Target	Angular distance	Position angle	Spectrograph aperture
CD (HRS)	0.215''	306°	0.22'' square
EF (HRS)	0.315''	30°	0.22'' square
Dsk 1 (HRS)	1.27''	321°	0.22'' square
Dsk 1 (FOS)	1.35''	321°	0.26'' circ
Dsk 2 (HRS)	2.46''	316°	0.22'' square
Dsk 2 (FOS)	2.52''	316°	0.43'' circ
Dsk 3 (HRS)	3.23''	317°	0.22'' square

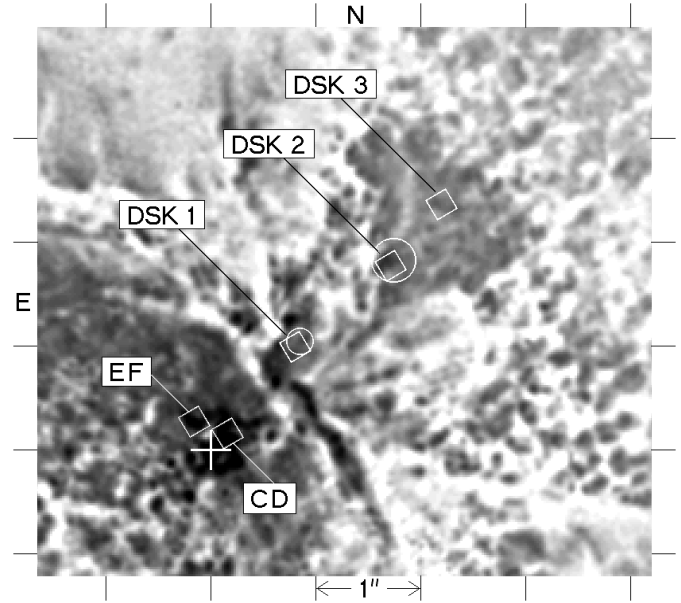
(3) Finally, and most interesting, *the equatorial ejecta may be restricted to a broad fan or sector about 120° wide, on the side of the Homunculus that faces toward us*; Fig. 1b certainly conveys this impression. A binary model with an eccentric orbit might produce such an effect by triggering asymmetric mass ejection near periastron. In such a model the ejecta are probably close to the bipolar midplane, so again one expects $\psi \approx 35^\circ$ for the material of interest here.

In summary, the true shape of the equatorial ejecta is ambiguous but the direction of motion near the projected bipolar axis is close to $\psi \approx 35^\circ$ in likely models. The uncertainty is difficult to assess, as noted in Sect. 5 below. With this likely value of ψ , at our observed position “Dsk 1” (see below) the heliocentric doppler velocity of ejecta from the Great Eruption seen in the 1840’s would be about -135 km s^{-1} , and the value for material ejected 50 years later would be almost -200 km s^{-1} . At locations farther out, of course, faster speeds would be expected.

3. The observations, and the general character of the spectrum at each location

We observed several appropriate positions in 1996 and 1997 with the HST’s Goddard High Resolution Spectrograph (HRS) and Faint Object Spectrograph (FOS). The target locations are listed in Table 1 and shown in Fig 2. This paper concerns mainly the three positions labeled “Dsk,” signifying “equatorial disk” although we have no proof that they are accurately in the midplane of the bipolar configuration. Since locations Dsk 1–3 are roughly superimposed on the projection of the bipolar axis northwest of the star, they probably represent that sector of the equatorial structure which is expanding most nearly in the direction toward us. Positions CD and EF were observed for other purposes and are included in Table 1 for the sake of completeness; they include the slow-moving “Weigelt blobs” C, D, E, and F which are located only about 1000 a.u. from the star (Weigelt et al. 1995, Davidson et al. 1997).

For each set of observations the central star was located by a careful peakup and then used as a reference for positional offsets. With the HRS this procedure was exactly as described in Davidson et al. (1997). With the FOS, a tiny 0.1'' aperture was used for the peakup on the star, referring only to a wavelength interval near 4800 Å which is dominated by continuum; this choice minimized contamination by emission lines produced

**Fig. 2.** Positions observed with the HRS and FOS, as listed in Table 1. Dsk 1–3 are in the “northwest fan” visible directly above the star in Fig. 1.

in ejecta about 0.2'' from the star. A few minor inconsistencies occurred in our target acquisitions, mainly due to a lack of information in 1995 when the observations were planned. For instance, Dsk 1 and Dsk 2 were observed with both the HRS and the FOS, but the positions differed slightly for the two instruments because we erroneously expected the initial HRS peakup reference point to be slightly northwest of the central star. Dsk 1 does not coincide with a single bright condensation, because imaging data in that region were inadequate when we chose the target location. These positional defects are nearly harmless for the results described in this paper; indeed they fortuitously led to the inclusion of three interesting and distinct velocity components in the data at position Dsk 1. Relative positions listed in Table 1 are based on analyzes of all the spectroscopic data as well as improved WFPC2 images, and should be accurate within 0.03''.

Our HRS and FOS observations were made on 1996 September 5 and 1997 February 7, respectively. (The latter date was only a few days before these instruments were removed from the HST.) Since the FOS data are merely supplemental background information so far as this paper is concerned, we note only that the “FOS/BL” detector was used with gratings G190H, G270H, G400H, and G570H to sample wavelengths between 1600 and 5500 Å, and statistical noise levels were much smaller than the weakest lines of interest at wavelengths longer than about 2500 Å. The HRS observations are more important here. Following an acquisition procedure like that described in Davidson et al. (1997), data were obtained with HRS detector 2 and the small HRS aperture, a 0.22'' square oriented at a position angle of about 30° during these observations. With HRS grating G270M we sampled wavelength intervals about 45 Å wide centered near 2450, 2500, and 2845 Å; the spectral resolution was

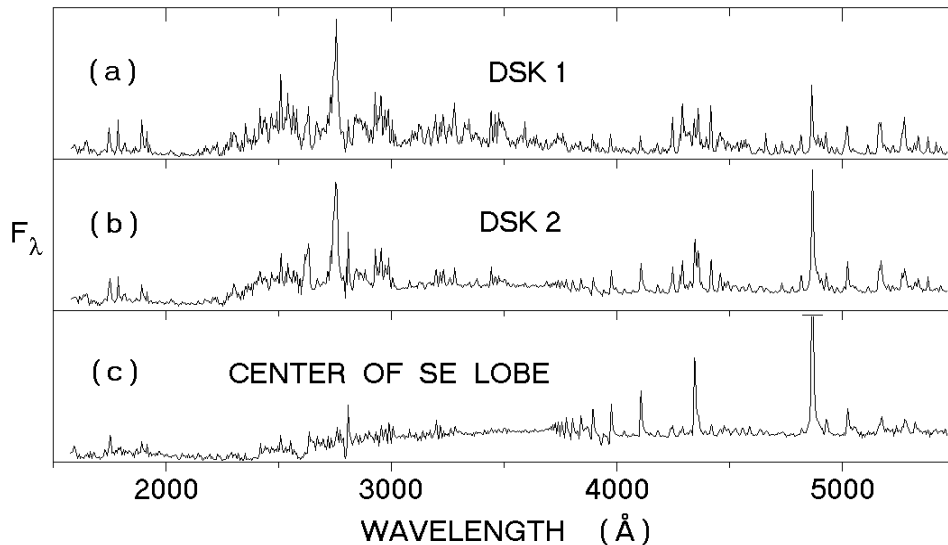


Fig. 3a–c. Spectra at positions Dsk 1, Dsk 2, and at a place 4 arcsec south-east of the central star, observed with FOS. Flux through the FOS aperture is shown with no corrections for extinction or aperture throughput, but the vertical scales differ among the three tracings. Almost all the spectral features seen here are real; at wavelengths longer than 2500 Å, statistical noise in these data is too small to see at this scale. Spectrum **c** in the Homunculus lobe is essentially a reflection of the central star, with almost no intrinsic emission by local gas. Spectra **a** and **b** in the equatorial region are dominated by emission lines produced at the observed positions, especially at UV wavelengths.

Table 2. HRS integration times

Target	Central wavelength				
	1748 Å	1904 Å	2452 Å	2502 Å	2845 Å
CD	352 s	272 s	120 s	120 s	96 s
EF	–	–	–	144 s	104 s
Dsk 1	–	–	–	327 s	300 s
Dsk 2	–	–	–	490 s	463 s
Dsk 3	–	–	–	–	463 s

about 0.1 Å. For the brightest target we also used grating G160M to sample intervals 35 Å wide centered near 1750 and 1905 Å. The integration times are listed in Table 2. The major line components described in Sect. 4 below had several thousand counts each; in most cases, statistical noise is only a minor contributor to the overall uncertainty in each observed wavelength.

The Homunculus is often said to be essentially a reflection nebula whose visual-wavelength spectrum resembles that of the central object (see refs. cited by Davidson and Humphreys 1997). However, the FOS data plotted in Fig. 3 show that this is not true for the “equatorial” material of interest here, northwest of the star. Parts (a) and (b) of Fig. 3 represent positions Dsk 1 and Dsk 2 in this region. Part (c) of the figure, on the other hand, shows the spectrum of a place in the southeast lobe of the Homunculus, 4 arcsec southeast of the star, observed in 1996 as part of a different FOS project. At least in the wavelength interval 2700–5400 Å, Fig. 3c is indeed a reflection of the star, with no discernible emission lines produced by ejecta outside the stellar wind. (For FOS data on the stellar wind itself, excluding the nearby ejecta that contaminate ground-based spectroscopy, see Davidson et al. 1995.) Figs. 3a and 3b are obviously different from 3c: They are dominated by a forest of narrow Fe II, Ni II, Cr II, and [Fe II] emission lines, excited both collisionally and radiatively. Position Dsk 1, especially, is brightest at near-UV wavelengths; this suggests that the local extinction by dust is not severe there, and may explain the violet glow in that

vicinity evident in WFPC2 images (see Morse et al. 1998). The reflected spectrum of the star is weak at position Dsk 1.

The most conspicuous UV features at Dsk 1 and Dsk 2 have unresolved peaks near 2750 and 2757 Å in the FOS data; they are due to Fe II λ 2750.13 and λ 2756.55 (UV 63, λ_{vac}) and their excitation has not yet been analyzed. Not knowing during the planning process that they are so bright, we did not include them in the HRS observations. Closer to the star, at positions CD and EF, these features are not conspicuous and the very peculiar Fe II fluorescent lines near 2507 and 2509 Å are far brighter as noted below. Regarding the overall spectrum at CD, see Davidson et al. (1995, 1997).

Thus the spectra at Dsk 1, Dsk 2, CD, and EF differ from that of the star; moreover, their most prominent emission lines are narrower than any features in the star’s spectrum. Therefore our HRS observations discussed below refer almost entirely to intrinsic emission produced at those locations, not reflected light.

Throughout this paper we quote vacuum wavelengths and heliocentric Doppler-shift velocities, except where otherwise stated. Spectroscopic designations for most emission lines are omitted in the text, but listed in Table 7.

4. Features and velocities found in the HRS data

We shall focus our attention on locations Dsk 1, Dsk 2, and Dsk 3 because they are pertinent to the equatorial-velocity question. The HRS data at those places are dominated by narrow emission lines, which in the following discussion we divide into two groups: high-excitation Fe II fluorescence lines with upper levels around 11 eV pumped by the hydrogen Ly α line, and low-excitation Fe II, Cr II, and Ni II lines with upper levels around 5–6 eV. The reasons for treating these two groups separately will be evident below: they behave differently in the observed spectra. Typical line widths in the HRS data are around 25 km s $^{-1}$.

The pumping of certain Fe II levels by H Ly α photons has been discussed in papers by Johansson & Jordan (1984) and

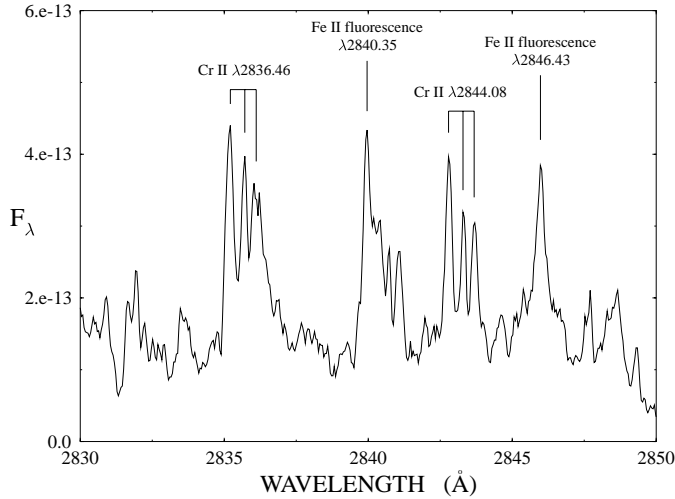


Fig. 4. The 2830–2850 Å region of the HRS Dsk 1 observation. The two Cr II UV 5 lines are split into three components, while the Fe II fluorescence lines appear as single peaks. The $\lambda 2840$ fluorescence line appears to have multiple components redwards of the main peak, corresponding to *redshifted* velocities, not seen for any other transition. These lines have, however, been identified as low-excitation Fe II lines, with velocities consistent with those found for the Cr II lines.

Johansson & Hamann (1993). $\text{Ly}\alpha$ photoexcitation from the $a^4\text{D}$ term of the Fe II ground configuration (about 1 eV above the ground level) results in significant populations of Fe^+ ions with energies about 11 eV above the ground state. The decay routes from these levels include various strong primary and secondary cascades, whose strength in observed spectra of stars like η Carinae, RR Tel and some symbiotic stars is difficult to explain by other mechanisms. A schematic view of these processes is shown in Fig. 7 of Johansson & Hamann (1993).

Previous HST observations of η Carinae have verified that fluorescence works very effectively in the dense “objects CD”, seen about $0.2''$ from the star (Davidson et al. 1995; Johansson et al. 1996; Davidson et al. 1997; Johansson et al. 1998). The two strongest observed UV features there are Fe II $\lambda 2507.552$ and $\lambda 2509.097$ (laboratory wavelengths, in vacuo). Their abnormal strengths and component ratios near η Carinae have been discussed by Johansson et al. (1996, 1998), who proposed that the ejecta act as a dichromatic ultraviolet laser. (This suggestion is extraordinary, and unique in astrophysics so far as we know. The photon and gas densities would certainly not lead one to expect much stimulated emission, but this is the only process suggested so far that plausibly explains why the two strongest lines are extremely intense while two other, closely related transitions from the same upper levels are not. Maybe path lengths with anomalously narrow velocity dispersions allow stimulated emission in the observed gas blobs. In any case, the fluorescent nature of the excitation is less controversial than the stimulated emission idea.)

Very strong radiation from UV multiplets 380, 391 and 399 (2800–2900 Å) confirms the radiative excitation process. These lines originate from the terms $e^4\text{D}$ and $e^6\text{D}$ about 10 eV above the ground state, and represent secondary fluorescence cascades.

Their upper levels are not directly photoexcited by the $\text{Ly}\alpha$ line, but are populated by primary cascades from the pumped 5p levels, observed in the near-IR spectrum (Johansson 1977, Johansson & Hamann 1993).

The low-excitation Fe II lines in the HRS data belong to various UV multiplets such as 175, 179, 207, 268 and 285. Their upper levels, e.g. $x^4\text{D}$, $x^4\text{F}$, $x^4\text{G}$ and $y^2\text{D}$, have excitation potentials between 7.5 and 8.5 eV. In addition to normal thermal excitation, these levels are probably populated by both continuum and discrete photoexcitation (see Johansson & Hamann 1993; Carpenter et al. 1988). Details of these processes are beyond the scope of this report and will be discussed in a later paper. The Cr II UV 5 multiplet is very prominent in our data; with upper levels near 6 eV, it may be thermally (collisionally) excited. The same is true for a strong Ni II line (UV multiplet 18) which is another of the strongest lines in our HRS observations.

4.1. Observed wavelengths and velocities

Observed wavelengths used in the following discussion refer to the peaks of emission lines. The 1-sigma uncertainty for each measurement is expected to be about $\pm 60 \text{ m}\text{\AA}$ or 6 km s^{-1} , including the effects of optical limitations, finite diode width in the HRS detector, and possible off-center positions in the HRS aperture. In this section we quote heliocentric apparent radial velocities; the systemic velocity of η Carinae, most likely around -7 km s^{-1} , will be taken into account later.

4.2. The lower-excitation lines; multiple velocity systems

The spectrum of Dsk 1 centered at 2850 Å contains 10 lines of the Cr II UV 5 multiplet. For nine of these lines we observe three separate, narrow components, indicating the presence of *three distinct velocity systems* at about -42 , -80 , and -136 km s^{-1} (heliocentric).

The line splitting is best illustrated by the two strongest lines in this Cr II multiplet, viz. $\lambda 2836.46$ and $\lambda 2844.08$, shown in Fig 4. The intensities of individual velocity components tend to decrease with increasing apparent wavelength. However, for other lines in the multiplet, no obvious correlation is seen between intensity and velocity. The $\lambda 2836.46$ line seems to have a fourth component, blueshifted by 26 km s^{-1} , but no counterpart is seen in any of the other Cr II lines.

Since the three velocities are narrow and distinct, one suspects that they originate in compact gaseous condensations. Fig. 5 shows that the region covered by the HRS aperture at Dsk 1 does include at least three such “blobs,” each with a characteristic size of the order of $0.05''$ or perhaps less ($< 3 \times 10^{15} \text{ cm}$). If these are the sources of the individual line components, we do not know which condensation is responsible for each velocity. Velocity errors of about $\pm 5 \text{ km s}^{-1}$ may result from the off-center placement of each blob in the HRS aperture. We are somewhat puzzled by the small sizes of these condensations and others like them, because reasonable expansion speeds should have led to larger sizes. Perhaps they are confined by pressure of lower-density faster ejecta flowing around them. (Fig. 5 is

Table 3. Cr II a⁶D - z⁶F observed at Dsk 1

Transition $J_{low} - J_{upp}$	λ_{lab} Å	λ_{obs} Å	$\Delta\lambda$	
			Å	km s ⁻¹
9/2–11/2	2836.46	2835.19	-1.27	-134
		2835.70	-0.76	-80
		2836.01	-0.45	-48
		2836.22	-0.24	-25
7/2–9/2	2844.09	2842.80	-1.29	-136
		2843.31	-0.78	-82
		2843.69	-0.40	-42
5/2–7/2	2850.67	2849.30	-1.37	-144
		2849.87	-0.80	-84
		2850.19	-0.48	-51
3/2–5/2	2856.51	2855.22	-1.29	-135
		2855.78	-0.73	-77
		2856.13	-0.38	-40
9/2–9/2	2859.75	2858.48	-1.27	-133
		2859.01	-0.74	-78
		2859.34	-0.41	-43
1/2–3/2	2861.77	2860.44	-1.33	-139
		2861.01	-0.76	-80
		2861.34	-0.43	-45
7/2–7/2	2863.41	2862.09	-1.32	-138
		2862.67	-0.74	-78
		2863.00	-0.41	-43
5/2–5/2	2865.94	2864.65	-1.29	-135
		2865.20	-0.74	-77
		2865.56	-0.38	-40
3/2–3/2	2867.58	2866.25	-1.33	-139
		2866.80	-0.78	-82
		2867.17	-0.41	-43
1/2–1/2	2868.49	2867.17	-1.32	-138
		2868.10	-0.39	-41

a simplified picture of the situation. The true HRS response is spatially blurred by about one-fourth the aperture size, while the precise aperture position may be uncertain by more than one-tenth the aperture width.)

Table 3 and Fig. 6 summarize the data for the Cr II features. The $\lambda 2850.67$ line is affected by a strong absorption feature, and has therefore been excluded from calculations of the average blueshifts. The line observed at 2867.17 Å may represent both Cr II $\lambda 2867.58$ at -43 km s⁻¹ and Cr II $\lambda 2868.49$ at -138 km s⁻¹, and was for this reason also excluded when determining the average velocities.

The Fe II energy level structure is such that many strong transitions occur at wavelengths around 2500 Å. Consequently the Dsk 1 spectrum centered at 2500 Å is crowded with low-excitation Fe II lines. Line blending therefore makes this spectrum more difficult to interpret. The observed wavelengths are less accurate than for the Cr II lines discussed above, and in some cases an observed feature has more than one possible identification. Nevertheless, the observed Fe II lines with positive identifications and reliable wavelengths have blueshifts consistent with

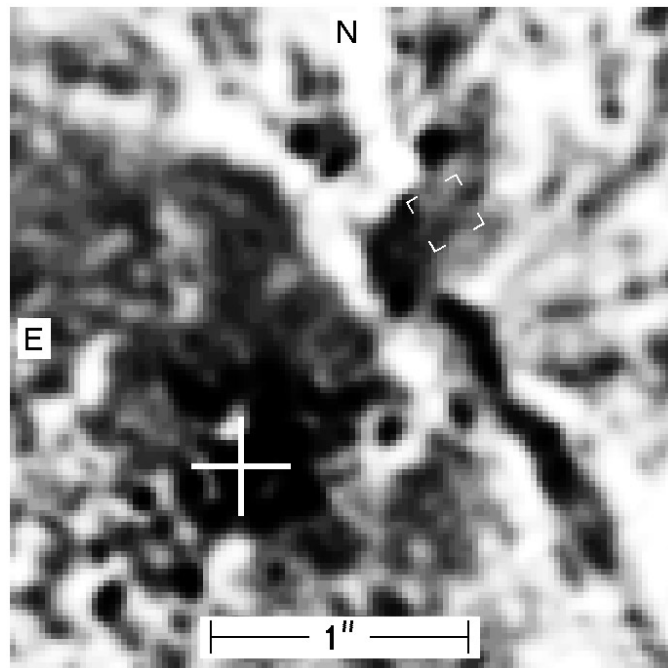


Fig. 5. Closer view of position Dsk 1 (cf. Fig. 3), showing that several discrete condensations were observed with the HRS. The precise position of the square HRS aperture is probably uncertain by roughly 15 percent of its width.

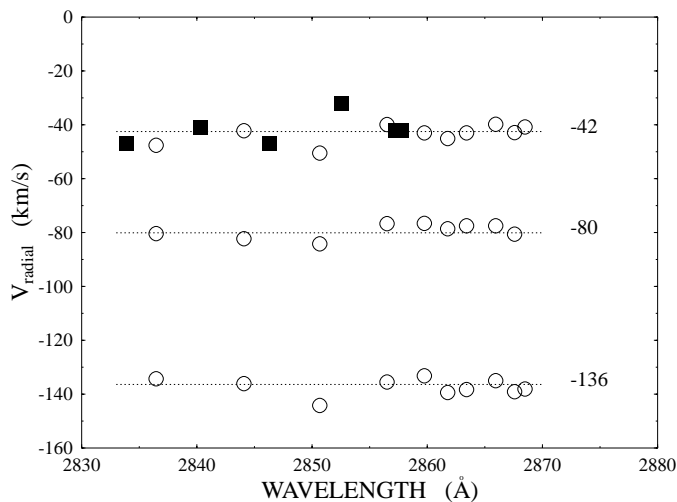


Fig. 6. Plot showing the observed velocities derived from the Cr II UV5 lines (circles) and the Fe II fluorescence lines (filled squares) in the Dsk 1 observation centered at 2850 Å.

those found for the Cr II lines, though not all three components are always seen. Examples are Fe II $\lambda 2480.91$ with three distinct components observed at -44 , -78 , and -136 km s⁻¹, and Fe II $\lambda 2521.85$ with two components at -39 and -137 km s⁻¹. The average radial velocities for identified Fe II lines near 2500 Å are -43 , -79 , and -138 km s⁻¹, in excellent agreement with those seen in the Cr II lines.

Excepting the 2507 – 2509 Å lines discussed below, the strongest feature in the 2500 Å observation at Dsk 1 is iden-

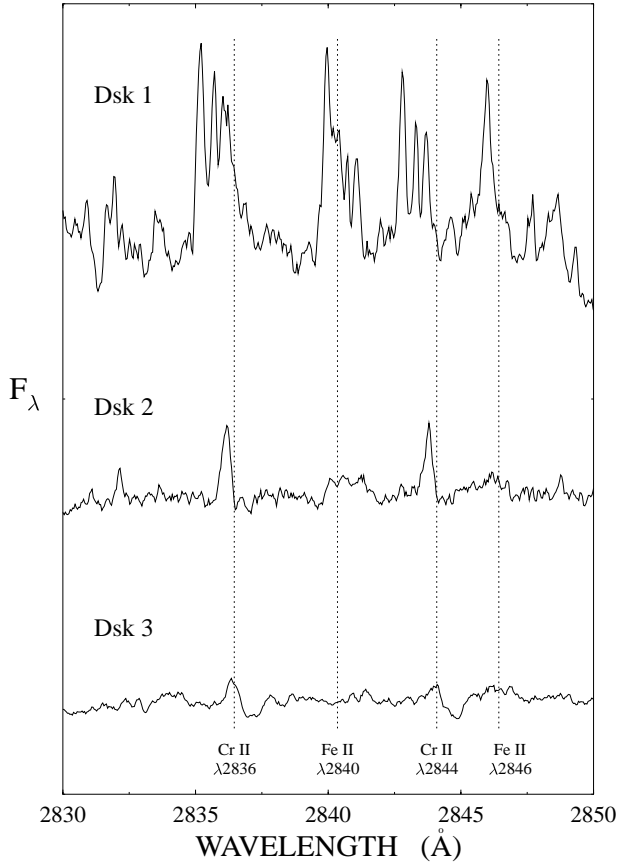


Fig. 7. The 2825–2850 Å region of the HRS spectra of Dsk 1, Dsk 2 and Dsk 3, showing the behavior of the low-excitation Cr II lines and the high-excitation Fe II fluorescence lines. The vertical intensity scale is the same for the three locations. The dotted lines mark the laboratory wavelength for each transition.

tified as Ni II $\lambda 2511.63$ (UV 18), blueshifted at -46 , -83 , and -139 km s $^{-1}$ (see Fig. 8).

One arcsec farther out in the equatorial disk, at position Dsk 2, the narrow emission lines are weaker. The strongest unblended lines of Fe II, Cr II, and Ni II are observed at blueshifts between -28 and -35 km s $^{-1}$, about 10 km s $^{-1}$ slower than the smallest velocity observed at Dsk 1. Some of the Cr II UV 5 lines have traces of the same three-component structure seen at Dsk 1, with weak features at roughly -80 and -140 km s $^{-1}$. The Cr II $\lambda 2844.08$ line, for example, has a main peak observed at 2843.80 Å, with a flux approximately 15 times larger than each of two weaker components seen at 2843.21 and 2842.75 Å.

At Dsk 3 the emission is even weaker. The strongest lines are blueshifted between -10 and -15 km s $^{-1}$. There are no signs of multiple velocity systems. Many pronounced absorption features are observed; the Cr II UV 5 lines, for example, have strong redshifted absorptions between $+65$ and $+85$ km s $^{-1}$. Similar absorptions are found for many of the low-excitation Fe II lines near 2500 Å. These may represent the spectrum of the stellar wind, redshifted because the dust grains that reflect it are moving outward. However, if this interpretation is correct, then the

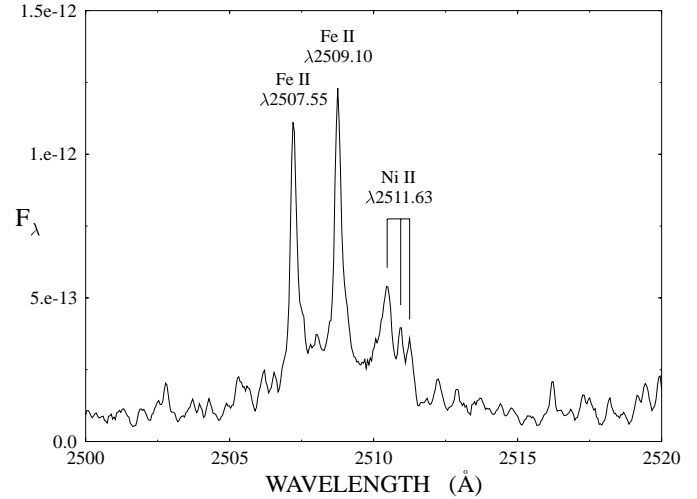


Fig. 8. The Fe II $\lambda 2507.55$ and $\lambda 2509.10$ fluorescence lines and the low-excitation Ni II $\lambda 2511.63$ as observed at Dsk 1. The fluorescence lines have only one component, while the Ni II line are split into three components with blueshifts similar to those of the Cr II UV5 lines. Also seen in this portion of the observed spectrum is a forest of weaker Fe II emission.

reflecting material is probably moving much faster than the gas that produces the weak narrow emission lines in the Dsk 3 data.

Fig. 7 shows a comparison of the spectra of Dsk 1, Dsk 2, and Dsk 3 near 2850 Å.

4.3. The fluorescence lines induced by Ly α

In the light of the data presented above, the presence of three different velocity systems at position Dsk 1 seems inarguable. However, *the high-excitation Fe II fluorescent lines appear only in the slowest of these systems.* This is true for both the primary and the secondary cascades that appear in the observed spectra. Moreover, the fluorescence lines are bright only in the spectrum of Dsk 1, are weak at Dsk 2, and cannot be seen at Dsk 3 farther from the central star.

Fe II $\lambda 2507.552$ and $\lambda 2509.097$ at Dsk 1, shown in Fig. 8, are observed at blueshifts of -40 and -41 km s $^{-1}$ respectively. The fluorescence lines with upper levels in the e 4 D and e 6 D terms (UV multiplets 380, 391 and 399), seen in the 2850 Å observation, show similar blueshifts, e.g., Fe II $\lambda 2840.35$ observed at 2839.96 Å (-41 km s $^{-1}$), $\lambda 2846.43$ seen at 2845.98 Å (-47 km s $^{-1}$), and $\lambda 2857.75$ observed at 2857.35 Å (-42 km s $^{-1}$). These velocities are in good agreement with the slowest velocity found for the low-excitation lines, and no signs of the faster components are seen. The strongest line observed in this wavelength region is at 2852.26 Å. We identify it as Fe II $\lambda 2852.56$, which, however, implies a blueshift of only -32 km s $^{-1}$, about 10 km s $^{-1}$ slower than the other fluorescence lines. This feature may be affected by strong interstellar Mg I $\lambda 2852.96$ absorption, but if so, its true velocity is even slower than -32 km s $^{-1}$.

At position Dsk 2 the fluorescence lines have almost disappeared from the observed spectra. The 2507–2509 Å lines are

Table 4. Fe II H Ly α fluorescence lines observed at Dsk 1

Transition	λ_{lab} Å	Dsk 1	
		λ_{obs} Å	$\Delta\lambda$ km s $^{-1}$
$c^4F_{7/2} - ({}^5D)5p \ 6F_{9/2}$	2507.55	2507.20	-42
$c^4F_{7/2} - (b^3F)4p \ 4G_{9/2}$	2509.10	2508.75	-42
$z^6P_{5/2} - e^6D_{5/2}$	2833.92	2833.47	-48
$z^4F_{9/2} - e^4D_{7/2}$	2840.35	2839.96	-41
$z^4F_{7/2} - e^4D_{5/2}$	2846.43	2845.98	-47
$z^4F_{3/2} - e^4D_{1/2}$	2852.56	2852.26	-32
$z^6P_{5/2} - e^6D_{7/2}$	2857.22	2856.82	-42
$z^4D_{7/2} - e^4D_{7/2}$	2857.75	2857.35	-42

Table 5. Ejection speeds and apparent ages

Location	V_{obs} (km s $^{-1}$) ^a	V_{ej} (km s $^{-1}$)	likely age, yr	2σ range ^b , yr
Dsk 1	-42	39±10	620	320–1450
Dsk 1	-81	87±12	280	165–520
Dsk 1	-136	154±17	160	100–280
Dsk 2	-30	< 40	–	> 1000
Dsk 2	-80	90±13	530	300–1000
Dsk 2	-140	160±18	290	175–520
Dsk 3	-12?	< 30	–	> 1500

^a Standard errors in the observed heliocentric radial velocities are probably about ± 6 km s $^{-1}$ for Dsk 1, perhaps a little worse for Dsk 2 and Dsk 3.

^b Errors in the estimated ages since ejection are generally dominated by uncertainty in the viewing angle ψ which is assumed to be $35^\circ \pm 7^\circ$. Each age and value of V_{ej} listed here is valid only if the observed component is in the “equatorial” zone of the ejecta structure, which is probable but unproven. Deceleration is assumed to be negligible, see remarks in the text. For the slowest cases, the uncertain systemic velocity of η Carinae is also important.

still seen, but are far less prominent than at Dsk 1. Their peaks at 2507.35 and 2508.95 Å correspond to Doppler velocities of -24 and -18 km s $^{-1}$ respectively, even slower than the low-excitation lines mentioned in Sect. 4.2. Some of the e^4D and e^6D lines near 2850 Å are also faintly visible. Their radial velocities are more uncertain but appear to be between -22 and -31 km s $^{-1}$. At Dsk 3, scarcely a trace of the fluorescent lines can be seen.

The fluorescence lines observed at Dsk 1 and Dsk 2 are summarized in Table 4.

4.4. Velocities at CD and EF

Position CD close to the star has been discussed before (Davidson et al. 1997), and EF is northeast rather than northwest of the star, so it is not close to the projected bipolar axis (see Tables 1 and 2). However, let us mention the velocities found there, as parenthetical background information. These condensations are denser and more intense than Dsk 1–3. At CD, as reported in the earlier paper, the fluorescent lines have doppler velocities around -47 km s $^{-1}$, consistent with ejection about 100 years

ago, while the Cr II lines have smaller blueshifts, possibly because of absorption on their short-wavelength edges.

At location EF, reflected light from the star is relatively stronger: the fluorescence lines are much weaker than at CD, and the emission lines are broader, with narrow peaks superimposed in some cases. Fe II $\lambda 2507.552$ is split into two components, one at -42 km s $^{-1}$ and the other *redshifted* at $+13$ km s $^{-1}$. The companion $\lambda 2509.097$ line has three components at -47 , -22 , and $+17$ km s $^{-1}$. In each case the redshifted component is strongest. The other fluorescent lines as well as the lower-excitation Fe II and Cr II lines at EF have the same appearance: each has a redshifted component between $+10$ and $+24$ km s $^{-1}$ and some have one or two weaker blueshifted components. Geometrical ambiguities make this situation difficult to interpret, but our tentative guess is that one of these “Weigelt blobs,” either E or F, is on the far side of the slow debris within 1500 a.u. ($\sim 2 \times 10^{16}$ cm) of the star.

5. Implications

As noted in Sects. 1 and 2, we expected to observe a doppler velocity near -200 km s $^{-1}$ at position Dsk 1, and higher speeds at Dsk 2 and Dsk 3. The results are quite different and raise a number of interesting problems:

- (1) Were the apparently slow-moving condensations ejected long before the famous Great Eruption seen in the 1840’s?
- (2) If so, then why did η Carinae, whose typical wind speeds are several hundred km s $^{-1}$, eject material at speeds much less than 100 km s $^{-1}$?
- (3) Why do the gas condensations have such small internal velocity dispersions? They are impressively compact (Fig. 2 and Fig. 5).
- (4) Why are certain fluorescent Fe II lines bright only in the slowest gas condensations? (A possibly relevant fact: Cox et al., 1995, have reported millimeter-wave maser emission at heliocentric radial velocities of about -40 km s $^{-1}$ in the ejecta close to the star.)

We must postpone questions (3) and especially (4) to later papers, but (1) and (2) deserve immediate comments. Table 5 is a list of ejection speeds V_{ej} and “ages” (elapsed times since ejection), indicated by the HRS data under the simplest set of assumptions. These have been calculated from

$$V_{ej} = -\frac{V_{obs} - V_{system}}{\cos \psi}$$

and

$$t = \frac{b}{V_{ej} \sin \psi},$$

where b and ψ are the projected distance from the star and the viewing angle defined in Sect. 2 above. In Table 5 we adopt a distance of 2300 pc and a systemic velocity of -7 km s $^{-1}$ for η Carinae, and we assume that the ejecta have not been decelerated.

The worst source of uncertainty in each estimated “age” is usually the viewing angle $\psi \approx 90^\circ - i \approx 35^\circ$ as noted in Sect. 2

Table 6. Viewing angles ψ for assumed ages of 100 and 150 years

Location	V_{obs} (km s $^{-1}$)	If $t = 100$ yr:		If $t = 150$ yr:	
		ψ	V_{ej} (km s $^{-1}$)	ψ	V_{ej} (km s $^{-1}$)
Dsk 1	-42	76 \pm 5 $^\circ$	145	69 \pm 5 $^\circ$	100
Dsk 1	-81	62 \pm 4 $^\circ$	160	51 \pm 4 $^\circ$	120
Dsk 1	-136	47 \pm 4 $^\circ$	190	36 \pm 4 $^\circ$	160
Dsk 2	-30	85 \pm 3 $^\circ$	270	83 \pm 3 $^\circ$	180
Dsk 2	-80	75 \pm 3 $^\circ$	280	68 \pm 3 $^\circ$	195
Dsk 2	-140	64 \pm 3 $^\circ$	300	53 \pm 3 $^\circ$	220
Dsk 3	-12	89 \pm 3 $^\circ$	350	89 \pm 3 $^\circ$	235

above. Almost all estimates of the Homunculus inclination angle i , based on various data and on more than one line of reasoning, have been between 50 $^\circ$ and 60 $^\circ$ (see refs. cited by Davidson & Humphreys 1997). This general agreement suggests that the true inclination is likely to be within that range with a probability, we guess, of 70 percent or better; which leads to an informal “pseudo-sigma” error estimate of $\pm 5^\circ$ for i . We also adopt the same uncertainty for the departure of the observed gas from the equatorial midplane; therefore, in Table 5, ψ is assumed to be $35^\circ \pm 7^\circ$. If the observed gas is indeed equatorial material, this error estimate is justified in the sense that errors as large as $\pm 14^\circ$ would be surprising. Then the fastest velocity observed at Dsk 1 is consistent with ejection in the Great Eruption, but *all the other velocities seem to represent earlier events with rather small ejection speeds*. Let us return to this point after noting alternative interpretations that may invalidate the “age” estimates proposed in Table 5.

In one alternative view, suppose that the observed spectra do not represent the equatorial plane; then the viewing angles ψ can be much larger than 35 $^\circ$. In Table 6 we list the values of ψ and V_{ej} that would be consistent with ages t of either 100 or 150 years. The -81 km s $^{-1}$ velocity component in Dsk 1 and the -140 km s $^{-1}$ component in Dsk 2 have $\psi \sim 50^\circ$ or 60° in Table 6, corresponding to latitudes around 20 $^\circ$ in the bipolar configuration. These two gaseous condensations may be on the surface of the northwest bipolar lobe, viewed through the equatorial disk. However, most of the other velocity components require $\psi > 70^\circ$ if their ages are 150 years or less, placing them *inside* the lobe.

This would be surprising in several ways. Since the low-latitude parts of the dusty lobes are suspected to be optically thick at visual and UV wavelengths, we do not expect to see material inside them. Low wind velocities make sense in the equatorial zones (see comments below), but not inside the polar lobes. If the lowest-speed velocity components represent gas inside the northwest lobe, why do they exhibit a different set of fluorescent lines? Moreover, the values of ψ for Dsk 3 and the -30 km s $^{-1}$ component in Dsk 2 are suspiciously close to the plane of the sky. Altogether, if some of the observed condensations are inside the northwest lobe, then they represent a new class of ejecta for η Carinae, posing new problems for the intermediate-latitude zones of the star. The non-equatorial hypothesis is a possible explanation for the low radial veloci-

ties in our data, but it is probably not the simplest one. Similar comments can be made regarding the possibility that we have seriously overestimated the system inclination angle i .

An anonymous reviewer of this paper has proposed an interestingly definite summary of one main result: *The special fluorescent emission lines cannot be formed in equatorial ejecta with ages less than 200 years*. This assertion is fairly robust in the sense that it remains true over the plausible range of inclination angles.

Fortunately, observable proper motions of condensations can provide a straightforward test of the “age” question in the foreseeable future, independent of the angle ψ . Proper motions of condensations near Dsk 2 and Dsk 3 are expected to be of the order of 0.02'' yr $^{-1}$ for material ejected 100–150 years ago, and slower, of course, for earlier ejection dates. These rates are of the order of 0.5 pixel per year with the HST/WFPC2(PC) instrument. High-quality WFPC2(PC) images of the Homunculus now span an interval of about 3 years (1994–1997), probably not long enough for this purpose; but a time baseline of 5 or 6 years, say, would make a test feasible if careful analysis techniques are employed. Some of the apparent projected distances between condensations northwest of the star are expected to change discernibly if they have different ages as our HRS data suggest.

In principle, a second way to invalidate Table 5 is to invoke possible deceleration of the observed gas since it was ejected from the star. But this would not explain much; it would require the presence of a larger mass of even slower-moving material. Since the idea of deceleration merely transfers the problem to another, hypothetical, unobserved mass of material, this is not the first hypothesis one should try.

Tentatively, at least, the most straightforward attitude is to assume that Table 5 is basically correct, and that distinct gaseous condensations were ejected from the star at low speeds before the Great Eruption. The idea of earlier ejection events in η Carinae is not new; some faint condensations outside the Homunculus may have ages of several hundred years, based on their proper motions (Walborn et al. 1978, 1988). However, since deceleration has been suspected for those outer objects, our HRS results considerably strengthen the case for pre-1800 outbursts. If their deceleration is not large, the outer condensations labeled “W” and “E1–E2” by Walborn et al. have an apparent age of roughly 700 years. This may conceivably be related to the slowest velocity component at our observed position Dsk 1 and the intermediate component at Dsk 2 (Table 5).

We believe that *the low ejection speeds indicated by our data are significant clues to the physical structure of η Carinae*. Conceptual models of this object have usually involved much higher speeds of 300 to 800 km s $^{-1}$, which obviously characterize the bipolar lobes produced by the Great Eruption as well as emission-line profiles in the present-day stellar wind (see many refs. cited in Davidson & Humphreys 1997). Wind speeds in that range seem reasonable for an evolved, very massive, moderately hot star. Why, then, do some well-defined condensations in the ejecta have speeds less than 100 km s $^{-1}$? A plausible working model can be based on rotation in combination with radiation

Table 7. Individual Cr II, Fe II and Ni II lines mentioned in this paper

Line	λ_{vac} (Å)	Transition	E_{upper} (eV)
Fe II	2480.91	$b^4F_{9/2} - x^4D_{7/2}$	7.80
Fe II	2507.55	$c^4F_{7/2} - ({}^5D)5p \ 6F_{9/2}$	11.17
Fe II	2509.10	$c^4F_{7/2} - (b^3F)4p \ 4G_{9/2}$	11.16
Fe II	2521.85	$a^2F_{5/2} - y^2D_{3/2}$	8.34
Fe II	2750.13	$a^4D_{5/2} - z^4F_{7/2}$	5.55
Fe II	2756.55	$a^4D_{7/2} - z^4F_{9/2}$	5.48
Fe II	2840.35	$z^4F_{9/2} - e^4D_{7/2}$	9.85
Fe II	2846.43	$z^4F_{7/2} - e^4D_{5/2}$	9.90
Fe II	2852.56	$z^4F_{3/2} - e^4D_{1/2}$	9.96
Fe II	2857.75	$z^4F_{7/2} - e^4D_{7/2}$	9.85
Cr II	2836.46	$a^6D_{9/2} - z^6F_{11/2}$	5.92
Cr II	2844.08	$a^6D_{7/2} - z^6F_{9/2}$	5.88
Cr II	2850.67	$a^6D_{5/2} - z^6F_{7/2}$	5.86
Cr II	2867.58	$a^6D_{3/2} - z^6F_{3/2}$	5.82
Cr II	2868.49	$a^6D_{1/2} - z^6F_{1/2}$	5.81
Ni II	2511.63	$a^2F_{7/2} - z^4G_{9/2}$	6.62

pressure. The following scenario may be roughly correct, but even if it is not, we hope that it suggests or inspires concrete alternatives. In the absence of rotation, the star's effective surface gravity g_{eff} is reduced by a factor $(1 - \Gamma)$, where Γ , the customary relative allowance for radiation pressure, is thought to exceed 0.7 or even 0.8 for η Carinae. If rotation at angular speed Ω is taken into account, the factor becomes $(1 - \Gamma - \Lambda)$ at the equator, where $\Lambda \approx \Omega^2 R^3 / GM$. A modest value of Λ causes a reduction in the equatorial value of g_{eff} and the star becomes slightly oblate. As a consequence, however, the surface temperature tends to decrease in the equatorial zone, which causes the local atmospheric opacity to increase, so that Γ is locally increased. (This effect is related to a hypothetical "Modified Eddington Limit" often proposed for LBV stars, see Sect. 5.2 of Humphreys & Davidson 1994.) The resulting decrease in $(1 - \Gamma)$ near the equator magnifies the relative importance of the centrifugal term Λ . Carried to its logical conclusion, this reasoning suggests that g_{eff} can be *substantially* reduced at the equator by rotation even if Λ is quite small. Since stellar wind and ejection speeds tend to be indirectly related to gravitational escape speeds, a reduction in the equatorial g_{eff} probably implies low ejection speeds there.

The qualitative model described above is obviously consistent with our assumption that the observed ejecta at positions Dsk 1–3 are essentially equatorial. Note also that the slow "Weigelt blobs" CD near the star are almost certainly near the equatorial midplane, based on a comparison of radial velocities with observed proper motions (Davidson et al. 1997, Weigelt et al. 1995). Moreover, various authors have reported spectroscopic hints that the wind of η Carinae is not spherically symmetric (cf. Viotti et al. 1989, Davidson et al. 1995, Ebbets et al. 1997). It is difficult to guess whether the hypothetical low-gravity equatorial zone exists most of the time or only during eruption events. If it is usually present, then η Carinae may be surrounded by a semi-permanent thick disk of diffuse ejecta.

This type of model can be modified in at least two obvious ways. First, the dynamically most relevant layers of the star may be below the photosphere (cf. Stothers & Chin 1993, 1994; Glatzel & Kiriakidis 1993). Second, the effect of a close companion star would have some characteristics in common with rotation in this situation (cf. comments in Sect. 5.5 of Humphreys & Davidson 1994; Davidson et al. 1997; Gallagher 1989).

Finally, as we noted above at the beginning of this section, a simple rotational model for low-speed ejection fails to make even qualitative contact with two major puzzles: We do not know why the slow ejecta are seen as dense, compact condensations, and worse, we cannot account for the fact that fluorescent excitation processes seem to occur only in the slowest velocity components. Problems like this deserve a great deal of theoretical attention.

Acknowledgements. We wish to thank the scheduling and instrument-specialist personnel at STScI, whose work is seldom easy when non-routine observations are required. T.Z. and S.J. acknowledge financial support from the Swedish National Space Board and the Crafoord Foundation. We are also grateful to Jon Morse, who has prepared high-quality images and maps of the Homunculus nebula that are wonderful resources for research on η Carinae.

References

- Carpenter K.G., Pesce J.E., Stencel R.E., et al., 1988, ApJS 68, 345
Cox P., Martin-Pintado J., Bachiller R., et al., 1995, A&A 295, L39
Currie D.G., Dowling D.M., Shaya E.J., Hester J.J., Scowen P., et al., 1996, AJ 112, 1115
Davidson K., Ebbets D., Weigelt G., et al., 1995, AJ 109, 1784
Davidson K., Humphreys R.M., 1997, ARA&A 35, 1
Davidson K., Ebbets D., Johansson S., et al., 1997, AJ 113, 335
Duschl W.J., Hofmann K.-H., Rigaut F., Weigelt G., 1995, Rev. Mex. Astron. Astrofis., Ser. Conf. 2, 17
Ebbets D.C., Walborn N.R., Parker J.W., 1997, ApJ 489, L161
Gallagher J.S., 1989, In: Davidson K., Moffat A., Lamers H. (eds.) Physics of Luminous Blue Variables. IAU Colloq. 113, p. 185
Glatzel W., Kiriakidis M., 1993, MNRAS 263, 375
Humphreys R.M., Davidson K., 1994, PASP 106, 1025
Johansson S., 1977, MNRAS 178, 17P
Johansson S., Hamann F.W., 1993, Physica Scripta T47, 157
Johansson S., Jordan C., 1984, MNRAS 210, 239
Johansson S., Davidson K., Ebbets D., et al., 1996, In: Benvenuti P., Macchetto F.D., Schreier E.J. (eds.) Science with the HST. STScI/ST-ECF Workshop, p. 361
Johansson S., Leckrone D.S., Davidson K., 1998, In: Brandt J.C., Petersen C.C., Ake III T.B. (eds.) The Scientific Impact of the Goddard High Resolution Spectrograph. ASP Conf. Ser. 143, p. 155
Morse J.A., Davidson K., Bally J., et al., 1998, AJ 116, 2443
Smith N., Gehrz R., 1998, AJ 116, 829
Smith N., Gehrz R., Krautter J., 1998, in preparation
Stothers R., Chin C.W., 1993, ApJ 408, L85
Stothers R., Chin C.W., 1994, ApJ 426, L43
Viotti R., Rossi L., Cassatella A., Altamore A., Baratta G.B., 1989, ApJS 71, 983
Walborn N.R., Blanco B.M., 1988, PASP 100, 797
Walborn N.R., Blanco B.M., Thackeray A.D., 1978, ApJ 219, 498
Weigelt G., Albrecht R., Barbieri C., et al., 1995, Rev. Mex. Astron. Astrofis., Ser. Conf. 2, 11